

Manuscript Number: HYDROL33849R1

Title: Exploring a Long Short-Term Memory based Encoder-Decoder Framework
for Multi-Step-Ahead Flood Forecasting

Article Type: Research paper

Keywords: Flood forecast; Encoder-Decoder (ED) model; Recurrent neural
network (RNN); Long short-term memory (LSTM); Sequence-to-sequence

Corresponding Author: Professor Fi-John Chang, PhD

Corresponding Author's Institution: National Taiwan University

First Author: I-Feng Kao, Ms

Order of Authors: I-Feng Kao, Ms; Yanlai Zhou, PhD; Li-Chiu Chang, PhD;
Fi-John Chang, PhD

Abstract: Operational flood control systems depend on reliable and accurate forecasts with a suitable lead time to take necessary actions against flooding. This study proposed a Long Short-Term Memory based Encoder-Decoder (LSTM-ED) model for multi-step-ahead flood forecasting for the first time. The Shihmen Reservoir catchment in Taiwan constituted the case study. A total of 12,216 hourly hydrological data collected from 23 typhoon events were allocated into three datasets for model training, validation, and testing. The input sequence of the model contained hourly reservoir inflows and rainfall data (traced back to the previous 8 hours) of ten gauge stations, and the output sequence stepped into 1- up to 6-hour-ahead reservoir inflow forecasts. A feed forward neural network-based Encoder-Decoder (FFNN-ED) model was established for comparison purposes. This study conducted model training a number of times with various initial weights to evaluate the accuracy, stability, and reliability of the constructed FFNN-ED and LSTM-ED models. The results demonstrated that both models, in general, could provide suitable multi-step ahead forecasts, and the proposed LSTM-ED model not only could effectively mimic the long-term dependence between rainfall and runoff sequences but also could make more reliable and accurate flood forecasts than the FFNN-ED model. Concerning the time delay between the time horizons of model inputs (rainfall) and model outputs (runoff), the impact assessment of this time-delay on model performance indicated that the LSTM-ED model achieved similar forecast performance when fed with antecedent rainfall either at a shorter horizon of 4 hours in the past (T-4) or at horizons longer than 7 hours in the past (> T-7). We conclude that the proposed LSTM-ED that translates and links the rainfall sequence with the runoff sequence can improve the reliability of flood forecasting and increase the interpretability of model internals.

Suggested Reviewers: Tanvir H. Bhuiyan PhD
Graduate Research Assistant, Civil & Environmental Engineering,
University of Louisville
tanvir.h.bhuiyan@gmail.com

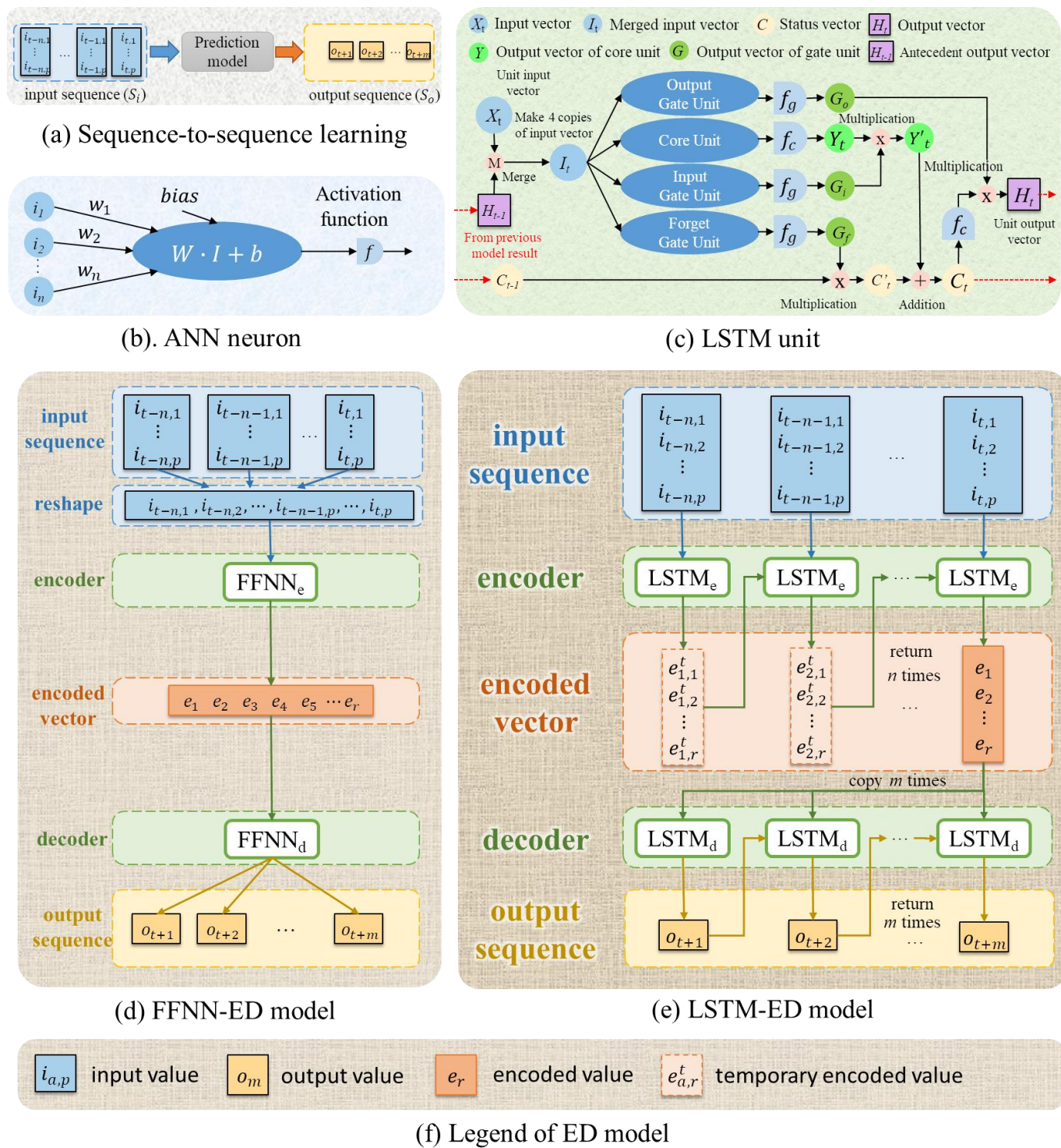


Figure 1 Architectures of the LSTM-ED and FFNN-ED models.

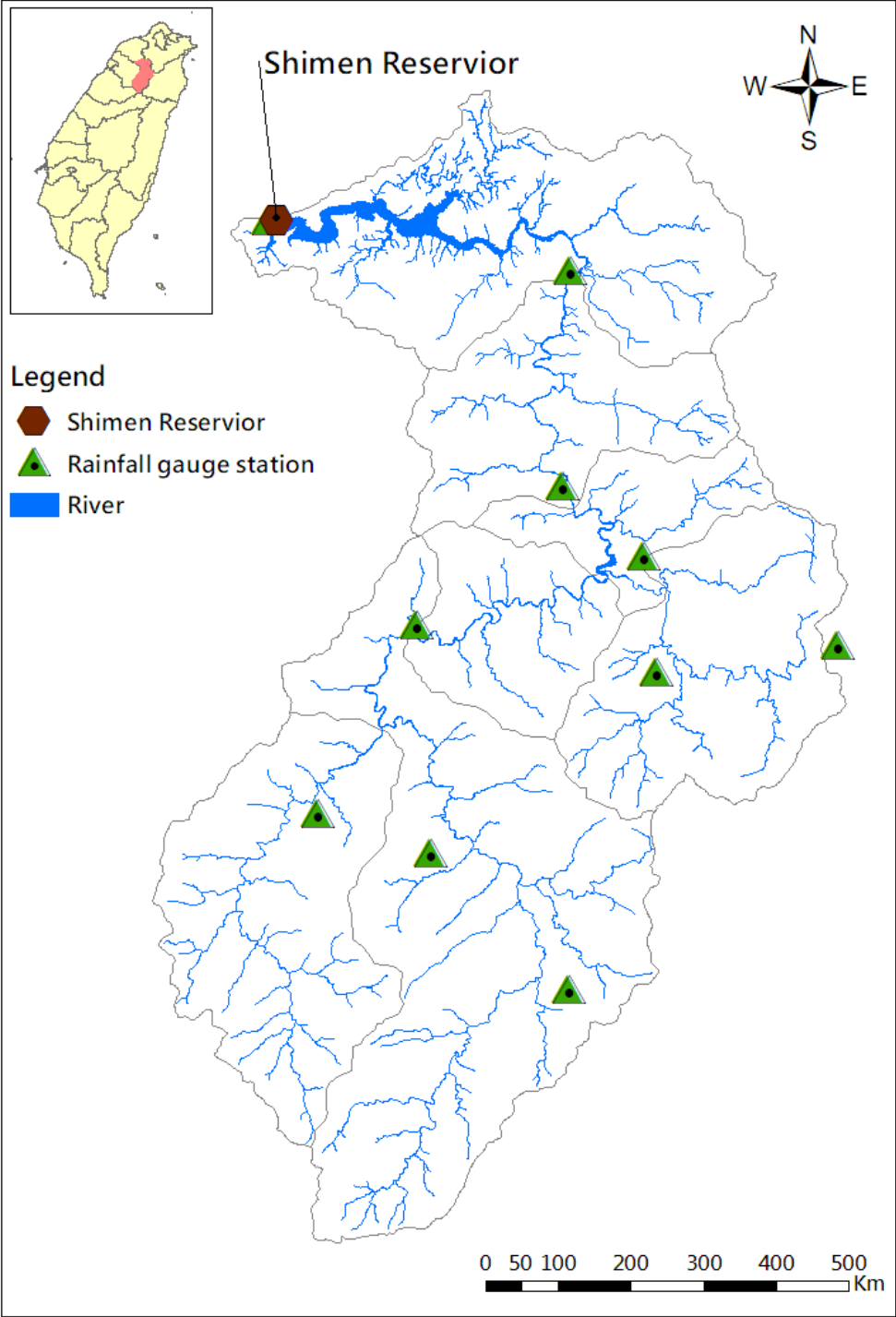
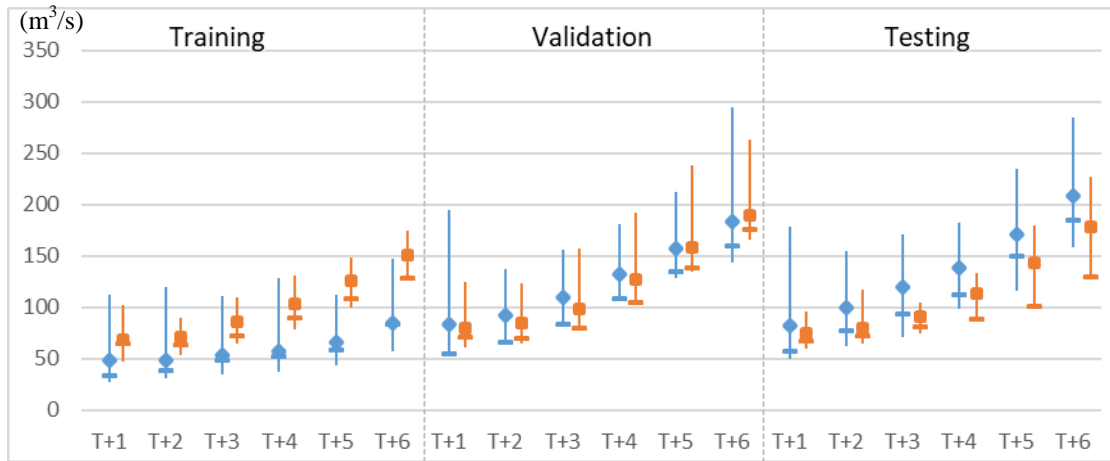
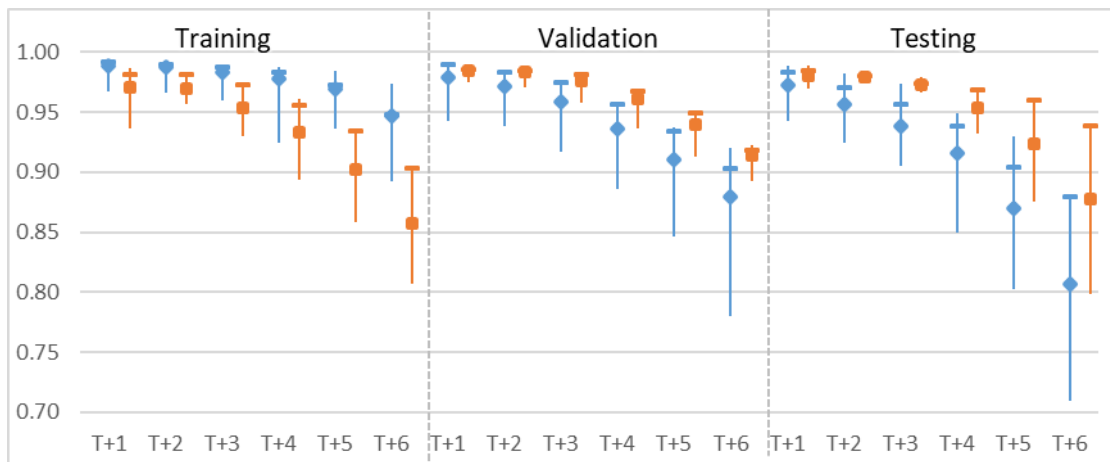


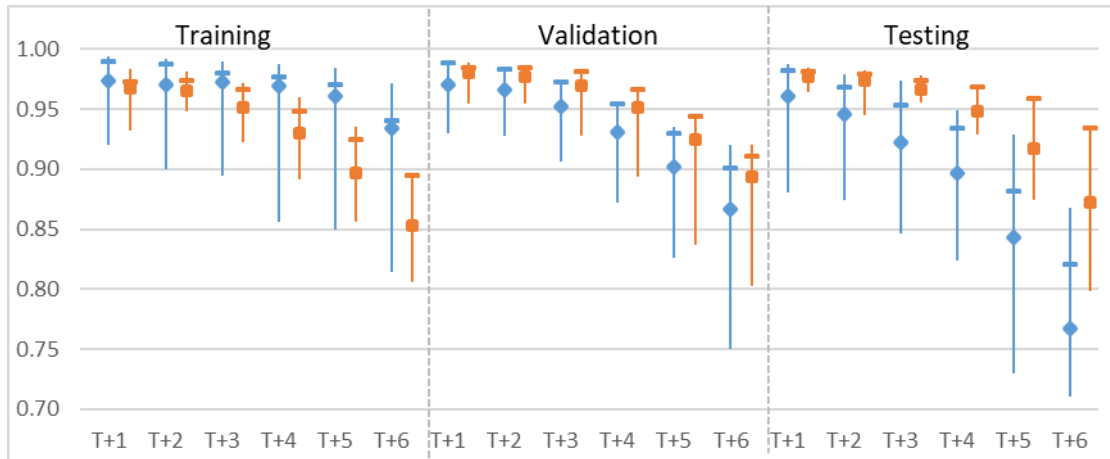
Figure 2 Locations of the Shihmen Reservoir catchment area and rainfall gauge stations.



(a) RMSE



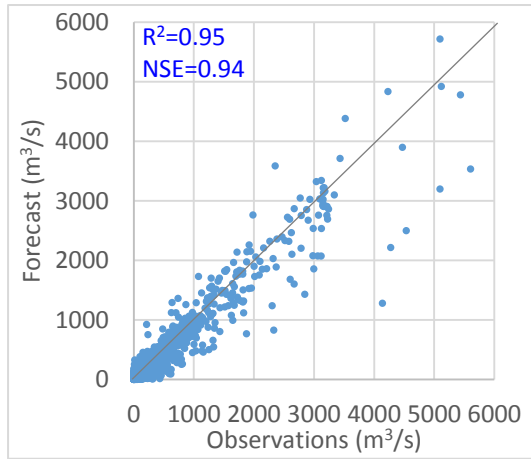
(b) R^2



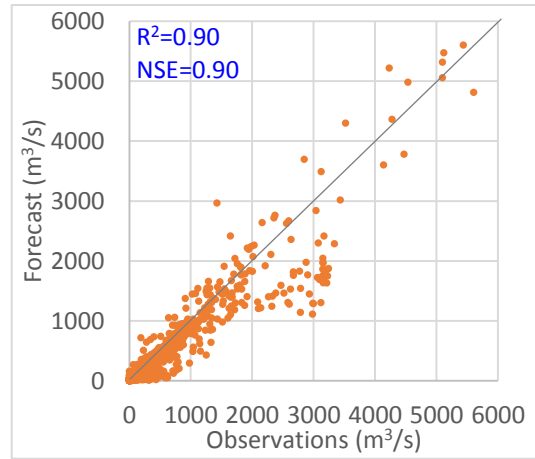
(c) NSE

FFNN-ED  LSTM-ED  Values of the best model 

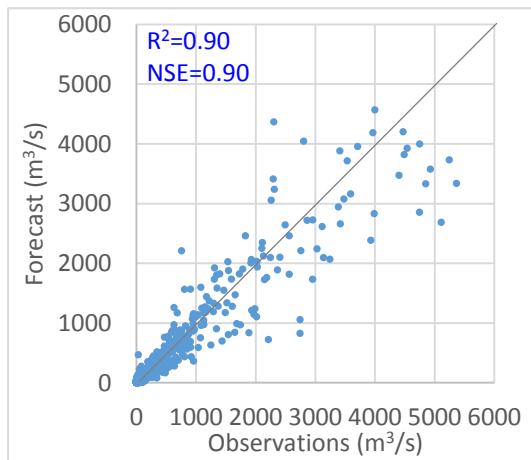
Figure 3 Performance of FFNN- and LSTM-ED models (each was performed 20 rounds). (a)-(c) RMSE, R^2 and NSE at horizons T+1–T+6, respectively. The range of an evaluation indicator is presented by a bar, where the mean and the value corresponding to best model are marked by a dot (diamond: FFNN-ED, and square: LSTM-ED) and a cross “+”, respectively.



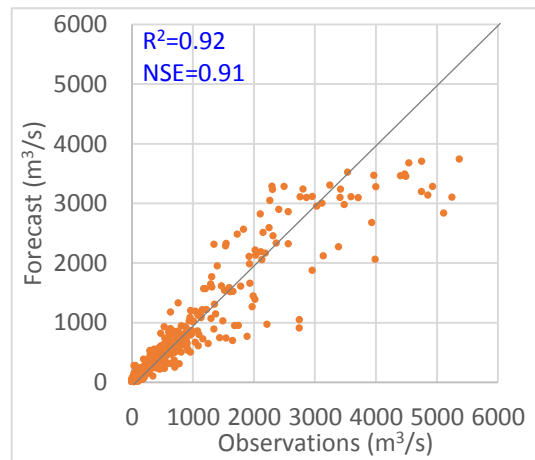
(a) FFNN-ED_training dataset



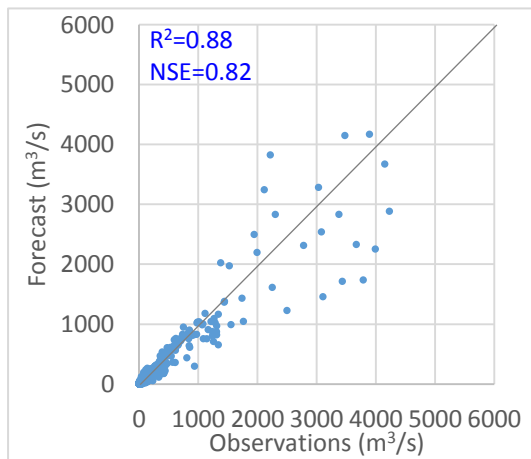
(b) LSTM-ED_training dataset



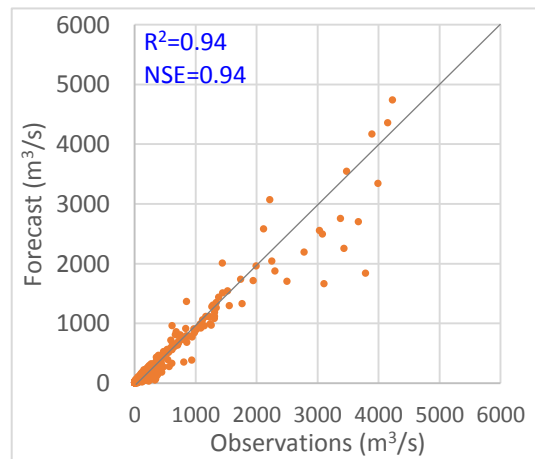
(c) FFNN-ED_validation dataset



(d) LSTM-ED_validation dataset



(e) FFNN-ED_test dataset



(f) LSTM-ED_test dataset

Figure 4 Scatter diagram of the best FFNN-ED and LSTM-ED models for T+6 forecasting.

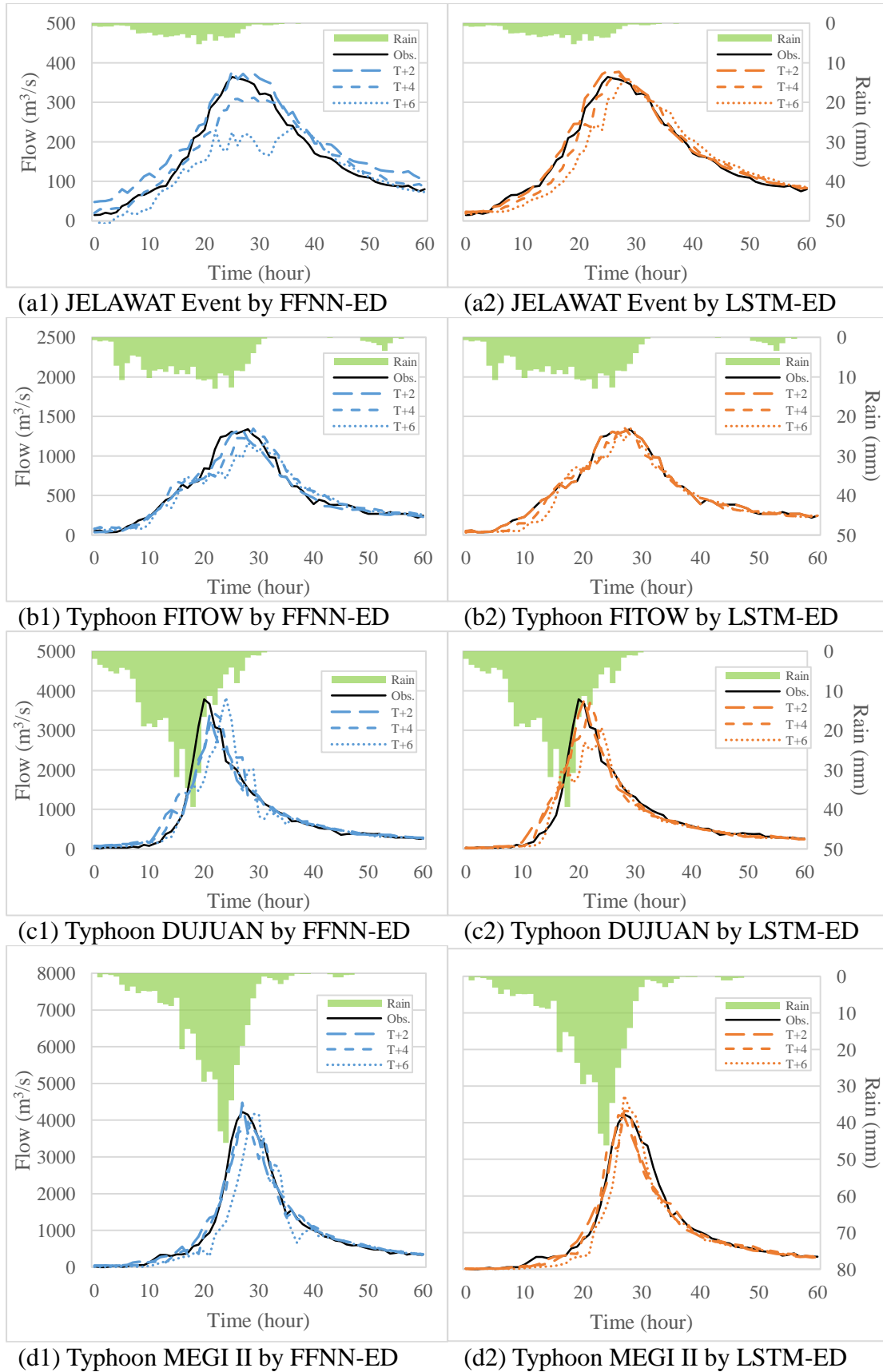


Figure 5 Comparison of observed and forecasted inflows obtained from the FFNN- and LSTM-ED models at horizons T+2, T+4 and T+6 for flood events corresponding to Typhoons JELAWAT, FITOW, DUJUAN and MEGI II.

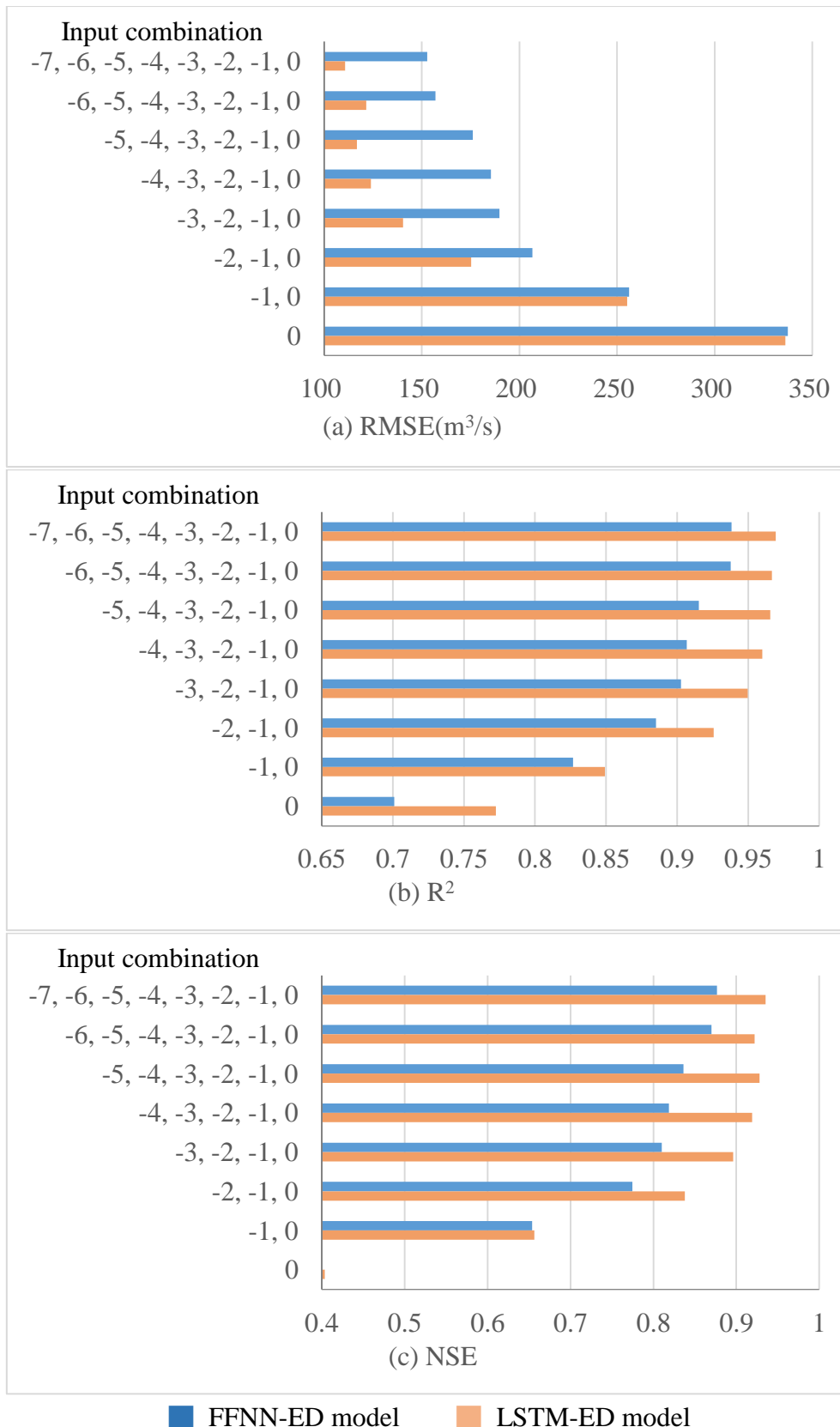


Figure 6 Performance of 6-step-ahead inflow forecasting using FFNN- and LSTM-ED models based on different numbers of antecedent (input) data, where 0 denotes data of the current time, and -n denotes data at horizon T-n (n=1-7, i.e. antecedent observed data). (a) RMSE. (b) R². (c) NSE.

Table 1 Typhoon events used in this study

Dataset	Typhoon	Max. inflow (m ³ /s)	Year	Duration
Training	SEPAT	1,844	2007	08/07 - 09/12
	SINLAKU	3,447	2008	09/11 - 09/26
	JANGMI	3,292	2008	09/26 - 10/18
	MORAKOT	1,827	2009	08/04 - 08/24
	FANAPI	1,059	2010	09/17 - 10/07
	MEGI 1	843	2010	10/16 - 11/07
	MEARI	1,060	2011	06/23 - 07/30
	SOULIK	5,458	2013	07/12 - 07/26
	TRAMI	2,410	2013	08/20 - 09/18
	MATMO	1,180	2014	07/21 - 08/22
	FUNG-WONG II	323	2014	09/19 - 10/24
	CHAN-HOM	917	2015	07/09 - 08/06
SOUDELOR	5,634	2015	08/06 - 09/12	
Validation	WIPHA	2,788	2007	09/17 - 10/02
	KROSA	5,300	2007	10/03 - 10/24
	FUNG-WONG	2,040	2008	07/26 - 08/08
	PARMA	616	2009	10/03 - 10/31
	SAOLA	5,385	2012	07/29 - 09/03
	USAGI	1,195	2013	09/18 - 10/05
Testing	JELAWAT	439	2012	09/27 - 10/07
	FITOW	1,393	2013	10/05 - 10/24
	DUJUAN	3,786	2015	09/27 - 11/03
	MEGI II	4,227	2016	09/26 - 10/02

Table 2 Performance of the FFNN- and the LSTM-based ED models at horizons T+1–T+6 for training, validation and test datasets.

Model	Dataset	Time step	RMSE		R ²		NSE	
			Mean (Max – Min)		Mean (Max – Min)		Mean (Max – Min)	
FFNN-ED	Training	T+1	48	(112 - 27)	0.99	(0.99 - 0.97)	0.97	(0.99 - 0.92)
		T+2	49	(120 - 31)	0.99	(0.99 - 0.97)	0.97	(0.99 - 0.90)
		T+3	53	(111 - 34)	0.98	(0.99 - 0.96)	0.97	(0.99 - 0.89)
		T+4	57	(129 - 38)	0.98	(0.99 - 0.92)	0.97	(0.99 - 0.86)
		T+5	65	(113 - 43)	0.97	(0.98 - 0.94)	0.96	(0.98 - 0.85)
		T+6	85	(147 - 57)	0.95	(0.97 - 0.89)	0.93	(0.97 - 0.81)
	Validation	T+1	83	(194 - 54)	0.98	(0.99 - 0.94)	0.97	(0.99 - 0.93)
		T+2	93	(137 - 69)	0.97	(0.98 - 0.94)	0.97	(0.98 - 0.93)
		T+3	109	(156 - 83)	0.96	(0.97 - 0.92)	0.95	(0.97 - 0.91)
		T+4	133	(182 - 106)	0.94	(0.96 - 0.89)	0.93	(0.96 - 0.87)
		T+5	157	(212 - 129)	0.91	(0.94 - 0.85)	0.9	(0.94 - 0.83)
		T+6	183	(295 - 144)	0.88	(0.92 - 0.78)	0.87	(0.92 - 0.75)
	Testing	T+1	83	(179 - 49)	0.97	(0.99 - 0.94)	0.96	(0.99 - 0.88)
		T+2	99	(155 - 62)	0.96	(0.98 - 0.92)	0.95	(0.98 - 0.87)
		T+3	120	(171 - 71)	0.94	(0.97 - 0.91)	0.92	(0.97 - 0.85)
		T+4	139	(183 - 98)	0.92	(0.95 - 0.85)	0.9	(0.95 - 0.82)
		T+5	171	(235 - 116)	0.87	(0.93 - 0.80)	0.84	(0.93 - 0.73)
		T+6	208	(285 - 158)	0.81	(0.88 - 0.71)	0.77	(0.87 - 0.71)
LSTM-ED	Training	T+1	59	(88 - 41)	0.97	(0.99 - 0.94)	0.97	(0.99 - 0.93)
		T+2	61	(77 - 46)	0.97	(0.98 - 0.96)	0.97	(0.98 - 0.95)
		T+3	74	(94 - 56)	0.96	(0.98 - 0.93)	0.95	(0.97 - 0.92)
		T+4	89	(112 - 67)	0.93	(0.96 - 0.89)	0.93	(0.96 - 0.89)
		T+5	108	(128 - 86)	0.9	(0.94 - 0.86)	0.9	(0.94 - 0.86)
		T+6	129	(150 - 110)	0.86	(0.90 - 0.81)	0.85	(0.90 - 0.81)
	Validation	T+1	68	(107 - 52)	0.99	(0.99 - 0.98)	0.98	(0.99 - 0.96)
		T+2	73	(106 - 56)	0.98	(0.99 - 0.97)	0.98	(0.99 - 0.96)
		T+3	85	(135 - 68)	0.98	(0.98 - 0.96)	0.97	(0.98 - 0.93)
		T+4	109	(165 - 89)	0.96	(0.97 - 0.94)	0.95	(0.97 - 0.9)
		T+5	137	(205 - 116)	0.94	(0.95 - 0.91)	0.93	(0.95 - 0.84)
		T+6	163	(226 - 143)	0.92	(0.92 - 0.89)	0.89	(0.92 - 0.8)
	Testing	T+1	64	(82 - 51)	0.98	(0.99 - 0.97)	0.98	(0.99 - 0.97)
		T+2	68	(101 - 56)	0.98	(0.99 - 0.98)	0.97	(0.98 - 0.95)
		T+3	78	(90 - 64)	0.97	(0.98 - 0.97)	0.97	(0.98 - 0.96)
		T+4	98	(115 - 76)	0.95	(0.97 - 0.93)	0.95	(0.97 - 0.93)
		T+5	123	(154 - 87)	0.92	(0.96 - 0.88)	0.92	(0.96 - 0.88)
		T+6	153	(195 - 111)	0.88	(0.94 - 0.80)	0.87	(0.94 - 0.80)

Table 3 Performance of the FFNN- and the LSTM-based ED models for flood forecasting at horizons T+2, T+4 and T+6 in the test dataset based on four typhoon-induced flood events at different scales.

Flood event	Time step	RMSE (m ³ /s)		R ²		NSE		Time shift in peak flow (hour)	
		FFNN	LSTM	FFNN	LSTM	FFNN	LSTM	FFNN	LSTM
JELAWAT ^a	T+2	42	20	0.93	0.96	0.80	0.96	0	0
	T+4	34	29	0.89	0.91	0.87	0.90	4	2
	T+6	51	40	0.79	0.83	0.70	0.82	12	3
FITOW ^b	T+2	43	25	0.99	0.99	0.96	0.99	-1	-1
	T+4	52	31	0.97	0.98	0.95	0.98	1	-1
	T+6	57	40	0.94	0.97	0.94	0.97	3	0
DUJUAN ^c	T+2	100	64	0.96	0.98	0.94	0.98	1	1
	T+4	111	89	0.94	0.96	0.93	0.96	2	2
	T+6	175	140	0.83	0.90	0.83	0.89	4	4
MEGI II ^d	T+2	133	145	0.98	0.98	0.98	0.97	0	-1
	T+4	118	164	0.99	0.97	0.98	0.97	1	0
	T+6	327	203	0.89	0.96	0.87	0.95	2	0

^a Typhoon JELAWAT with total rainfall of 67 mm and maximal flow of 439 m³/s.

^b Typhoon FITOW with total rainfall of 255 mm and maximal flow of 1,393 m³/s.

^c Typhoon DUJUAN with total rainfall of 413 mm and maximal flow of 3,786 m³/s.

^d Typhoon MEGI II with total rainfall of 443 mm and maximal flow of 4,227 m³/s.

1 **Exploring a Long Short-Term Memory based Encoder-Decoder Framework for**
2 **Multi-Step-Ahead Flood Forecasting**

3

4 I-Feng Kao^a, Yanlai Zhou^b, Li-Chiu Chang^c, Fi-John Chang^{a,*}

5 ^aDepartment of Bioenvironmental Systems Engineering, National Taiwan University, Taipei,
6 10617, Taiwan

7 ^b Department of Geosciences, University of Oslo, P.O. Box 1047 Blindern, N-0316 Oslo, Norway.

8 ^c Department of Water Resources and Environmental Engineering, Tamkang University, New
9 Taipei City, 25137, Taiwan

10 Correspondence to: Fi-John Chang (changfj@ntu.edu.tw)

11

12 **Abstract**

13 Operational flood control systems depend on reliable and accurate forecasts with a
14 suitable lead time to take necessary actions against flooding. This study proposed a
15 Long Short-Term Memory based Encoder-Decoder (LSTM-ED) model for
16 multi-step-ahead flood forecasting for the first time. The Shihmen Reservoir
17 catchment in Taiwan constituted the case study. A total of 12,216 hourly hydrological
18 data collected from 23 typhoon events were allocated into three datasets for model
19 training, validation, and testing. The input sequence of the model contained hourly
20 reservoir inflows and rainfall data (traced back to the previous 8 hours) of ten gauge
21 stations, and the output sequence stepped into 1- up to 6-hour-ahead reservoir inflow
22 forecasts. A feed forward neural network-based Encoder-Decoder (FFNN-ED) model
23 was established for comparison purposes. This study conducted model training a
24 number of times with various initial weights to evaluate the accuracy, stability, and
25 reliability of the constructed FFNN-ED and LSTM-ED models. The results
26 demonstrated that both models, in general, could provide suitable multi-step ahead

27 forecasts, and the proposed LSTM-ED model not only could effectively mimic the
28 long-term dependence between rainfall and runoff sequences but also could make
29 more reliable and accurate flood forecasts than the FFNN-ED model. Concerning the
30 time delay between the time horizons of model inputs (rainfall) and model outputs
31 (runoff), the impact assessment of this time-delay on model performance indicated
32 that the LSTM-ED model achieved similar forecast performance when fed with
33 antecedent rainfall either at a shorter horizon of 4 hours in the past (T-4) or at
34 horizons longer than 7 hours in the past ($> T-7$). We conclude that the proposed
35 LSTM-ED that translates and links the rainfall sequence with the runoff sequence can
36 improve the reliability of flood forecasting and increase the interpretability of model
37 internals.

38 **Keywords:** Flood forecast, Encoder-Decoder (ED) model, Recurrent neural network
39 (RNN), Long short-term memory (LSTM), Sequence-to-sequence

40

41 **1. Introduction**

42 Floods are one of the most dangerous natural disasters that notoriously threaten
43 human life and property. The International Centre for Water Hazard and Risk
44 Management (ICHARM) reported that floods accounted for about 30% of the total
45 natural disasters and affected more than 48% of people worldwide over the last
46 century (ICHARM, 2009). Floods are always a major concern in inundation prone
47 areas. This is especially true in Taiwan because there are, on average, three typhoons
48 to invade this island each year, and typhoon-induced heavy rainfalls usually cause
49 severe flood inundation in various cities near estuaries. Therefore, flood forecasting
50 plays a pivotal role in flood mitigation, floodplain management, agricultural
51 cultivation, and human life protection. The development of early warning systems for

52 flood defense encounters great challenges, which creates an outreach demand for
53 reliable and accurate multi-step-ahead forecasts. This pinpoints the focus of scientific
54 research for flood defense should be placed on increasing the reliability and accuracy
55 of forecast models at longer horizons.

56 Artificial neural networks (ANNs) can adequately mimic highly non-linear
57 complex systems and are widely used to tackle the modelling of complex systems in
58 hydrological fields (e.g. Dawson & Wilby, 2001; Chau, 2006; Kalteh et al., 2008;
59 Nourani et al., 2014; Chandwani, et al., 2015). For instance, precipitation or
60 evapotranspiration prediction (e.g., Shafaei et al., 2016; Shenify et al., 2016; Valipour
61 et al., 2016; Nourani et al., 2017; Nourani et al., 2020, Nourani et al.,2019), flood
62 forecasting (e.g., Chen et al., 2013; Chang et al., 2014; Lohani et al., 2014; Taormina
63 et al., 2015; Chang & Tsai, 2016; Noori & Kalin, 2016; Humphrey et al., 2016; Tan et
64 al., 2018), and rainfall-runoff modeling (e.g., Abrahart et al., 2007; Nourani &
65 Komasi, 2013; Badrzadeh et al., 2015; Nourani, 2017; Shoaib et al., 2018; Nourani et
66 al.,2018). Various studies also adopted ANNs for deploying hydrological prediction
67 during typhoons and storm events in Taiwan. For example, Tsai et al. (2014)
68 combined radar reflectivity and ground rainfall data to predict reservoir inflows using
69 the adaptive-network-based fuzzy inference system (ANFIS), and Chang et al. (2014)
70 used recurrent neural networks to make real-time multi-step-ahead flood forecasts for
71 a sewerage system in Taipei City.

72 The attractiveness of ANNs comes mainly from the remarkable characteristics of
73 data mining, such as learning ability, noise tolerance, and generalizability.
74 Nevertheless, different types of ANNs do have their own merits and limitations in
75 modeling complex systems. For instance, the feed forward neural network (FFNN)
76 fails to suitably manage time-series data because the state of the network is erased

77 after processing each data, i.e. information about the sequential order of the inputs is
78 discarded, which is not desirable when handling inherently interrelated data points.
79 Besides, the FFNN implements a fixed-sized sliding window protocol, which restrains
80 the model from learning or capturing the long-term dependencies between input and
81 output. On the other hand, recurrent neural networks (RNNs) are designed to capture
82 temporal dynamics by sequentially processing the inputs for modelling the nonlinear
83 relationship between input and output via cycles formed by the hidden nodes in the
84 network. In recent years, Deep Learning (DL) has gained a lot of attention. Deep
85 Neural Networks (DNNs) are powerful tools and achieve excellent performance on
86 difficult tasks (e.g., Sainath et al., 2015; Liu et al., 2017; Zhou et al., 2019). The long
87 short-term memory (LSTM) proposed by Hochreiter and Schmidhuber (1997) is a
88 type of DNNs configured with an RNN architecture. The LSTM is used to deal with
89 the exploding and vanishing gradient problems that may occur when training
90 traditional RNNs with long-term lags. Recently, LSTMs have been implemented to
91 explore its capability in time series forecasting of river flood (Le et al., 2019) and
92 water table depth (Zhang et al., 2018; Jeong & Park 2019) as well as to learn
93 long-term dependencies, e.g., storage effects within hydrological catchments (Kratzert
94 et al., 2018) and model rainfall-runoff processes (Sezen et al., 2019).

95 For neural networks, the sequence-to-sequence learning trains models by
96 converting sequences from one domain into another domain (Sutskever et al., 2014).
97 Sequence-to-sequence models have recently achieved significant performances on
98 complex tasks like machine translation, video to text, and question answering (Bengio
99 et al., 2015; Venugopalan et al., 2015; Wiseman et al., 2016; Chiu et al., 2018).
100 Sequence-to-sequence models configured with a LSTM unit have gained marvelous
101 achievements in various fields, like anomaly detection (Fengming et al., 2017), image

102 segmentation (Marmanis et al., 2018), video recognition (Zhu et al., 2017; Zhu et al.,
103 2018), machine translation (Audhkhasi et al., 2017; Malinowski et al., 2017;
104 Costa-Jussa, 2018), and air pollution forecasting (Freeman et al., 2018; Zhou et al.,
105 2019). From the perspective of data science, hydrological analyses involve many
106 physical processes similar to sequence-to-sequence problems. For instance,
107 rainfall-runoff processes can be considered as the conversion of rainfall sequences
108 into watershed discharge sequences. This provides merit to explore in-depth how the
109 rainfall sequence can be mapped onto a runoff sequence through DNN models for
110 reliably and accurately making multi-step-ahead flood forecasts.

111 This study proposes a LSTM-based Encoder-Decoder (LSTM-ED) model that
112 integrates a sequence-to-sequence learning, two LSTM units, and an
113 Encoder-Decoder scheme to make reliable and accurate multi-step-ahead flood
114 forecasts for the first time. In the beginning, the sequence-to-sequence learning is
115 employed to establish a multi-input and multi-output model structure. Then, the two
116 LSTM units and the sequence-to-sequence learning are fused into the
117 Encoder-Decoder scheme for constructing a multi-output deep learning neural
118 network (i.e., LSTM-ED). To demonstrate the applicability of the LSTM-ED model in
119 multi-step-ahead flood forecasting, this study utilizes an inflow series of the Shihmen
120 Reservoir in Taiwan as a case study. The remainder of this study is organized as
121 follows. Section 1 introduces the study background and makes a literature review.
122 Section 2 presents the framework of the proposed model. Section 3 introduces the

123 case study and materials. Section 4 presents the results and discussion of the methods
124 applied to multi-step-ahead flood forecasting. Conclusions are then drawn in Section
125 5.

126

127 **2. Methodology**

128 This study proposes a LSTM-ED model to improve the reliability and accuracy of
129 multi-step-ahead flood forecasts. For comparison, a feed-forward neural
130 network-based Encoder-Decoder (FFNN-ED) is also constructed. Fig. 1 illustrates the
131 architecture of the LSTM-ED and FFNN-ED models, where Fig. 1(a) presents the
132 sequence-to-sequence learning, Fig. 1(b) presents a prototype of an ANN neuron, Fig.
133 1(c) presents the LSTM unit, and Figs. 1(d) and 1(e) present the frameworks of the
134 LSTM-ED and FFNN-ED, respectively. The methods adopted in this study are briefly
135 introduced as follows.

136 **2.1 Sequence-to-sequence learning**

137 Sequence prediction is commonly centered on forecasting the succeeding value in an
138 observed sequence. Time series prediction problems usually concern either of the two
139 frameworks: 1) a sequence of one input time step converted to a sequence of one
140 output time step, or 2) a sequence of multiple input time steps converted to a sequence
141 of one output time step. It will be more challenging to make a sequence prediction

142 when taking a sequence as the input, which is termed as a sequence-to-sequence
 143 prediction problem. A sequence-to-sequence prediction problem involves an input
 144 sequence (S_i) and an output sequence (S_o). The input sequence contains known
 145 information, and the output sequence is the prediction target. Fig. 1(a) illustrates the
 146 sequence-to-sequence learning. Input and output sequences generally have different
 147 lengths, and the implementation process will require the entire input sequence as soon
 148 as the prediction of the target start. This study establishes a prediction model M to
 149 convert the input sequence into the output sequence. A sequence (S) is defined as a set
 150 of vectors (V_n) with time series relationship.

151 Definition 1: Sequence

$$S = \{V_1, V_2, \dots, V_n\} \quad (1)$$

$$V_x = \{v_{n,1}, v_{n,2}, \dots, v_{n,p}\} \quad (2)$$

152 where n is the length of the input time series (the lookback length of time) and p is the
 153 number of elements (variables) in a vector.

154 Definition 2: Prediction model

$$S_o = M(S_i) \quad (3)$$

155 In this study, the input sequences contain hourly data of ten rainfall gauge
 156 stations and the inflow data of the Shihmen Reservoir collected from the horizon $t-n$
 157 to the current time t . The output sequence is the multi-step-ahead reservoir inflow.
 158 That is to say, this study intends to establish a rainfall-runoff model for making
 159 reservoir inflow forecasts based on antecedent rainfall and inflow data.

160 Definition 3: rainfall-runoff model

$$S_i = \{I_{t-n}, I_{t-n-1}, \dots, I_{t-1}, I_t\} \quad (4)$$

$$I_t = \{i_{t,1}, i_{t,2}, \dots, i_{t,p}\} \quad (5)$$

$$S_o = \{O_{t+1}, O_{t+2}, \dots, O_{t+m}\} \quad (6)$$

$$t, p, n, m \in N \quad (7)$$

161 where I denotes a vector of the input sequence S_i , O denotes a vector of the output
 162 sequence S_o , t is the current time, n is the lookback length of time, m is the forecast
 163 horizon, and p is the number of gauge stations (rainfall or inflow in this study).

164 **2.2 Long short-term memory (LSTM) unit**

165 The LSTM units have several architectures. A common architecture comprises a core
 166 unit (the memory part) and three gate units (input, output and forget gates) that direct
 167 the information flow inside the LSTM unit (Fig. 1(c)). The computation steps of the
 168 LSTM are shown in Eqs. (8)-(16), referred from Hochreiter and Schmidhuber (1997).

169 (1) Combine the antecedent output vector with the input vector.

$$I_t = H_{t-1} + X_t \quad (8)$$

170 where I_t is the merged input vector that combines the antecedent output vector
 171 H_{t-1} with the input vector X_t .

172 (2) Calculate the output vector of the core unit.

$$Y_t = f_c(W_c \cdot I_t + b_c) \quad (9)$$

173 where Y_t and f_c are the output vector and the activation function of the core
 174 unit, respectively, W_c is the connection weight, and b_c is the bias of the core
 175 unit.

176 (3) Calculate the output vectors corresponding to the units of the input gate, the
 177 forget gate and the output gate.

$$G_i = f_g(W_i \cdot I_t + b_i) \quad (10)$$

$$G_f = f_g(W_f \cdot I_t + b_f) \quad (11)$$

$$G_o = f_g(W_o \cdot I_t + b_o) \quad (12)$$

178 where G_i , G_f and G_o are the output vectors (gate values) obtained from the
 179 input gate, forget gate and output gate units, respectively. The weights (W_i , W_f ,
 180 W_o) and bias (b_i , b_f , b_o) are the parameters corresponding to the three gate
 181 units. f_g denotes the activation function of a gate unit, and its output value falls
 182 between zero and one.

183 (4) Calculate the new cell state vector of long-term memory.

$$Y'_t = G_i \cdot Y_t \quad (13)$$

$$C'_t = G_f \cdot C_{t-1} \quad (14)$$

$$C_t = Y'_t + C'_t \quad (15)$$

184 where Y'_t is the raw output of the LSTM unit, and C'_t is the antecedent cell
 185 state vector (C_{t-1}) that is finely tuned by the forgot gate value (G_f). C_t is the
 186 new cell state vector of long-term memory, and it will return to the LSTM unit
 187 when being reused. In this step, the cell state vector of long-term memory gains
 188 new information but forgets some old information.

189 (5) Calculate the output vector of the LSTM unit.

$$H_t = f_c(C_t) \cdot G_o \quad (16)$$

190 where H_t is the output vector of the LSTM unit, and f_c is the same activation
 191 function as the one used in the core unit. The activation function can stabilize the
 192 output value after the LSTM unit are reused many times. The output gate value
 193 (G_o) can control whether the LSTM unit should produce an output or not. In
 194 addition, the cell state vector is not affected by f_c in this step such that it is
 195 much easy to keep the raw output (Y'_t) of this LSTM unit for the next reuse.

196 **2.3 Encoder-Decoder model**

197 Encoder-Decoder (ED) models have been developed to effectively tackle the challenging
198 sequence-to-sequence prediction problems lately. From the perspective of model
199 architecture, an ED model has two implementation phases: the first is to read the input
200 sequence and encode it into a fixed-length vector, and the second is to decode the
201 fixed-length vector and output the predicted sequence. The innovation of the ED
202 model is that the model facilitates a fixed-sized internal representation such that input
203 sequences are read to and output sequences are read from. It was noticed that an ED
204 model configured with LSTM was developed to cope with natural language
205 processing problems and achieved state-of-the-art performance in the text translation
206 field. This study intends to implement the ED architecture for translating the rainfall
207 sequence into the runoff sequence, where the lengths of the input sequence and the
208 output sequence are fixed. The two ED models with different encoders and decoders
209 are introduced as follows.

210 **2.3.1 FFNN-ED model**

211 Fig. 1(d) illustrates the structure of the FFNN-ED model, which uses the FFNN in the
212 encoder and decoder schemes. The input sequences are reshaped to a 1-dimensional
213 vector before entering the encoder. Then the encoder generates a 1-dimensional
214 encoded vector (error vector) and feeds it to the decoder. Finally, the decoder
215 produces a 1-dimensional vector of the output sequence. It is noted that the FFNN-ED
216 model serves as a comparative model in this study.

217 **2.3.2 LSTM-ED model**

218 The structure of the proposed LSTM-ED model is shown in Fig. 1(e). This study
219 utilizes the LSTM unit in the encoder and decoder schemes for improving the learning
220 of the continuity in input and output sequences. The LSTM unit will be reused many

221 times for “reading” the input sequence and “writing” the output sequence sequentially.
222 The numbers of times to reuse the LSTM units in encoding and decoding schemes
223 depend on the lengths of the input sequence and the output sequence, respectively. For
224 the encoding phase, the LSTM unit serves as a “collector” for accumulating rainfall
225 information. The LSTM unit can well simulate the physical mechanism of the
226 rainfall-runoff process, as shown in the previous studies (e.g., Kratzert, et al., 2018).
227 The process of reading a vector in the input sequence one-by-one is similar to the way
228 that rain falls to the ground sequentially. Integrating information through the recurrent
229 architecture is similar to the concentration of river flow with a time lag. Discarding
230 the previous input information by the forget gate (i.e., the LSTM computation step (4)
231 in Section 2.2) is similar to the hydrological phenomenon of precipitation loss and
232 infiltration during the rainfall-runoff process. When the encoder reads a vector, the
233 LSTM unit will generate a temporary encoded vector. The encoding process will
234 repeat n times so that all the input vectors enter the LSTM to produce their
235 corresponding encoded vectors. For the decoding phase, the LSTM unit generates the
236 output value of forecasted discharge (i.e., the reservoir inflow) sequentially. The input
237 to the LSTM unit during the decoding phase is a vector that merges the final encoded
238 vector and the output value (reservoir inflow) of the previous LSTM. It is noted that
239 the currently observed reservoir inflow is used to produce the output value of the
240 LSTM at horizon of 1 hour ahead ($T+1$) because there is no antecedent forecasted
241 reservoir inflow at the beginning of the decoding phase. The recurrent and sequential
242 processes (features) of the decoding phase that generates the output sequence is
243 similar to the continuity of river flow in a watershed. The LSTM unit fed with the
244 previous flow information can maintain the continuous feature of flows, which is not
245 available in the FFNN unit of the FFNN-ED model. The advantage of the LSTM-ED

246 model is that it can produce more stable and less fluctuated output values. Therefore,
 247 This study expects the LSTM-ED model can perform better than the FFNN-ED
 248 model.

249 **2.4 Evaluation of model performance**

250 This study adopts the root mean square error (RMSE), the coefficient of
 251 determination (R^2), and the Nash–Sutcliffe model efficiency coefficient (NSE) to
 252 evaluate the forecast results of the two ED models. The RMSE value represents the
 253 error between the forecasted and the observed values, and its unit is the same as the
 254 output value of the model. The RMSE value ranges from 0 to infinity. A model with
 255 its RMSE value closer to 0 implies that it can produce more accurate forecasts. The
 256 RMSE can be calculated by the following equation.

$$\text{RMSE} = \sqrt{\frac{1}{N} \sum_{t=1}^N (d_i - y_i)^2} \quad (17)$$

257 where N is the number of samples, d_i is the target output value, and y_i is the model
 258 output value.

259 The R^2 value is the proportion of the variance in the dependent variable that is
 260 predictable by the independent variable(s), and it is commonly used to evaluate the
 261 linear correlation between model outputs and target outputs. The R^2 value ranges from
 262 0 to 1. A model with its R^2 value closer to 1 implies it can predict more accurately.

263 The R^2 value can be calculated by the following equation.

$$R^2 = \left[\frac{\sum_{t=1}^N (d_i - \bar{d})(y_i - \bar{y})}{\sqrt{\sum_{t=1}^N (d_i - \bar{d})^2 \sum_{t=1}^N (y_i - \bar{y})^2}} \right]^2 \quad (18)$$

264 where \bar{d} is the mean of target outputs, and \bar{y} is the mean of model outputs. Other
 265 symbols are consistent with those of Eq. (17).

266 The NSE is commonly used to evaluate hydrological prediction models. The
267 NSE value ranges from negative infinity to 1. A model with NSE value closer to 1
268 implies it can predict more accurately. A model with its NSE value less than 0 reveals
269 it performs worse than a model that produces mean values only. The NSE value can
270 be calculated by the following equation.

$$\text{NSE} = 1 - \frac{\sum_{t=1}^N (d_i - y_i)^2}{\sum_{t=1}^N (d_i - \bar{d})^2} \quad (19)$$

271 where all the symbols are consistent with those of Eqs. (17) and (18).

272

273 **3. Case study and materials**

274 **3.1 Study area**

275 The Shihmen Reservoir basin with an area of 763.4 km² is located in northern Taiwan
276 (Fig. 2). It has an annual average rainfall of 2,504 mm and an annual inflow of 1.47
277 billion m³. In this basin, 76% of rainfall occurs within six months (May-October),
278 with a high incidence of typhoon events (Water Resources Agency, Taiwan, 2016).
279 This is consistent with typical rainfall-runoff characteristics in Taiwan. |

280 **3.2 Observational data**

281 This study collected the monitoring records associated with 23 typhoon events
282 occurring from 2007 to 2016, including hourly rainfall data of ten rainfall gauge
283 stations and the inflow data of the Shihmen Reservoir. Table 1 shows the information
284 of typhoon events used in this study. A total of 12,216 hourly data were allocated into
285 three datasets for model training (8,232 from 13 events), validation (2,688 from 6
286 events), and testing (1,296 from 4 events). The training dataset was used to adjust
287 model parameters such as the weights and bias of the neural network. The validation
288 dataset was used to verify whether a model is undertrained or overfitting. The test
289 dataset was used to evaluate model performance.

290 **3.3 Model construction**

291 After data pre-processing, the observational data were organized into an input
292 sequence and an output sequence. According to historical rainfall-runoff data of this
293 basin, the longest flood propagation time was 8 hours. Therefore, the input sequence
294 contained reservoir inflows and hourly data (traced back to the previous 8 hours of the
295 current time) of ten rainfall gauge stations. Considering the demand for the flood
296 control of the Shihmen Reservoir, the output sequence stepped into 1- up to 6-
297 hour-ahead reservoir inflow.

298 The FFNN-ED model behaved in a similar way to the BPNN model with 30
299 neurons in the hidden layer (i.e., the length of the encoded vector), and it was trained
300 by the Levenberg-Marquardt optimizer using MATLAB 2018b. The number of
301 neurons was determined by trial and error. For comparison purposes, the length of the
302 encoder vector for the LSTM-ED model was also set as 30. The LSTM-ED model
303 was implemented in Python, where the Python library Keras and the Adam optimizer
304 compiling were used in the training stage, and the dropout regularization was adopted
305 to avoid overfitting.

306

307 **4. Results and discussion**

308 Three evaluation indicators were conducted to evaluate the performance of the
309 LSTM-ED and FFNN-ED models. To verify model reliability, this study also
310 evaluated the model performance of four test flood events. Finally, the impacts of the
311 number of antecedent observed data (model inputs) on model performance were
312 investigated.

313 **4.1 Evaluation of model performance**

314 It was worth mentioning that the structures of LSTM-ED and FFNN-ED models were

315 different, so as their training algorithms. Therefore, this study investigated the
316 effectiveness and reliability of both models. Considering the FFNN-ED model had no
317 recurrent structure, the Levenberg-Marquardt optimizer with the second-order training
318 characteristics was implemented because it could reduce errors faster than the
319 gradient descent optimizer with the first-order training characteristics. In contrast, the
320 LSTM-ED model has a complex recurrent structure, an optimizer (such as Adam)
321 with the first-order training characteristics can reduce the complexity of the training
322 algorithm and make the model easy to train. The first-order training algorithm,
323 however, required more iterations, and therefore the training time of the LSTM-ED
324 model was much longer than the FFNN-ED model. It is noticed that the computation
325 time of the LSTM-ED model is, on average, about 20 times longer than that of the
326 FFNN-ED model (Computer specifications: Intel i7-6700 CPU, 16GB Memory, and 1
327 TB Storage. FFNN-ED: Matlab 2018b, Levenberg-Marquardt Optimizer, and 3-5
328 minute training time per round. (2) LSTM-ED: Python 3.6 with Keras 2.2.4, Adam
329 Optimizer, and 60-100 minutes training time per run). The training time, however, is
330 not the main issue to prohibit the utilization of these models. According to the runtime
331 records of the test case, the computation time of the two constructed Encoder-Decoder
332 models (FFNN-ED and LSTM-ED) for on-line forecasting is less than 1 minute. This
333 study raised more concerns about the accuracy, stability, and reliability of the
334 constructed models instead. Therefore, both models were trained 20 rounds (with
335 different initial weights) using the training datasets, and then model performances
336 were evaluated by validation and test datasets. The best model of each framework was
337 determined as the model that produced the highest R^2 value averaging over six time
338 steps in the validation stages. Finally, the best FFNN-ED model was compared with
339 the best LSTM-ED model.

340 The results (maximum, minimum, and mean values over 20 rounds) of the
341 FFNN-ED and the LSTM-ED models at each of the six horizons in all three stages are
342 shown in Table 2 and Fig. 3. It appears that both models, in general, could be trained
343 almost perfectly, in terms of very small RMSE values and very high R^2 and NSE
344 values at each horizon in the training stages. In addition, the forecast errors of both
345 models increased as the forecast horizon increased, which was caused by the lack of
346 future rainfall information in the long forecast horizons. The results of performance
347 show that the FFNN-ED models, in general, perform better than the LSTM-ED
348 models in the training stages, but this is not the case in validation and testing stages
349 (in fact, their performances are quite the opposite). The FFNN-ED models produced
350 much larger error ranges than the LSTM-ED models in all three stages. For the
351 FFNN-ED models, their mean values of the RMSE in the validation and testing stages
352 at the six horizons are 50%–250% higher than those of the training stages. For the
353 LSTM-ED model, the RMSE values are only slightly higher in the validation and
354 testing stages than in the training stage. The results of performance showed that the
355 LSTM-ED model reduced forecast errors (RMSE) by 3% up to 38% in the testing
356 stages at horizons 1 to 6 hours ahead (T+1–T+6), as compared to the FFNN-ED
357 model. Fig. 3 explicitly presents the detailed results (maximum, mean, and minimum
358 over 20 rounds) of both models at each of the six horizons in all three stages. The
359 results (20 rounds) of the constructed LSTM-ED models are much more consistent
360 than those of the constructed FFNN-ED models. The results of performance also
361 showed that the LSTM-ED model produced higher R^2 and NSE values than the
362 FFNN-ED model, especially true at long horizons (> 2 hours) in the validating and
363 testing stages. These results support that the LSTM-ED model outperforms the
364 FFNN-ED model, in terms of model stability, reliability, and accuracy.

365 Fig. 4 shows the scatter diagrams of the best FFNN-ED and LSTM-ED models
366 for T+6 forecasting in the training, validating, and testing stages, respectively. The
367 results of T+6 forecasting show that both models, in general, fit well to the observed
368 data in all three stages, and the LSTM-ED model has better performance (in terms of
369 higher R^2 and NSE values and narrowly dispersed points) than the FFNN-ED model
370 in the validating and testing stages. This is especially true in the testing cases, as the
371 study can easily conclude that the LSTM-ED model can make more accurate T+6
372 forecasting, especially under the conditions of high flow (>2000 cms), than the
373 FFNN-ED model.

374 **4.2 Evaluation of model reliability**

375 According to the flood forecast results of the four test events shown in Table 3, the
376 LSTM-ED model is superior to the FFNN-ED model with respect to RMSE, R^2 , and
377 NSE values. The hydrographs (near the peak flow) of observations and model
378 forecasts at horizons T+2, T+4, and T+6 are illustrated in Fig. 5. The first flood event
379 induced by Typhoon JELAWAT (total rainfall < 67 mm, maximal inflow= 439 m³/s)
380 had the smallest magnitude. The performances of both models for this event, however,
381 are the worst, as compared to those of the other three test events. As shown in Figs.
382 5(a1) and 5(a2), both models under-estimated peak flows.

383 The second flood event induced by Typhoon FITOW was also a small-scale
384 flood event, which was considered less hazardous to the Shihmen Reservoir. Its
385 maximal flow was $1,393$ m³/s, and the accumulated rainfall in the basin during the
386 first 48 hours of the typhoon period was 255 mm. Figs. 5(b1) and 5(b2) indicate that
387 the LSTM-ED model performs better in flow peak at horizons T+2, T+4, and T+6.
388 Besides, the LSTM-ED model maintains similar performance at all the three forecast
389 horizons, yet the forecast error of the FFNN-ED model increases significantly.

390 Moreover, the LSTM-ED model can accurately forecast the peak flow, whereas the
391 FFNN-ED model underestimates the peak flow.

392 The third flood event induced by Typhoon DUJUAN was a large-scale flood
393 event, and it was considered moderately hazardous. Its maximal flow reached 3,225
394 m^3/s , and the accumulated rainfall in the basin during the first 48 hours of the typhoon
395 period achieved 389 mm. Because there were multiple peaks in the rainfall
396 distribution, the forecasts obtained from both models were unstable and undulate in
397 the rising limb of the flood. The forecast results of both models at horizons T+2, T+4,
398 and T+6 illustrated in Figs. 5(c1) and 5(c2) display unstable forecasts and multiple
399 peaks. The results of this flood event forecasting show that the forecasting at horizons
400 T+4, unexpectedly, performs better than the forecasting at horizons T+2 and T+6. It is
401 observed from Figs. 5(c1) and 5(c2) that the interval between peaks in the rainfall
402 distribution spans approximately 4 hours. This information may be the key to solving
403 flood forecasting problems suffering from multi-peak rainfall distribution, which will
404 be investigated in future research.

405 The fourth flood event caused by Typhoon MEGI II was a large-scale flood event,
406 and it was considered highly hazardous. Its maximal flow reached 4,227 m^3/s , and the
407 accumulated rainfall in the basin during the first 48 hours of the typhoon period
408 achieved 443 mm. Table 3 indicates that the LSTM-ED model is superior to the
409 FFNN-ED model at horizons T+2, T+4 and T+6. The RMSE value of the LSTM-ED
410 model was about 50% smaller than that of the FFNN-ED model at each horizon. In
411 addition, the R^2 and NSE values of the LSTM-ED model still exceeded 0.95 for all
412 the three horizons. Figs. 5(d1) and 5(d2) clearly show that the LSTM-ED model
413 produces more accurate forecasts of peak flow than the FFNN-ED model.

414 Overall, the LSTM-ED model not only can produce more accurate forecasts on

415 high flow, especially true for flood events induced by single-peak rainfall
416 distributions (e.g., MEGI II, FITOW), but also can produce more stable forecasts on
417 flood events of multi-peak rainfall distributions (e.g., JELAWAT, DUJUAN), as
418 compared with the FFNN-ED model. The FFNN-ED model could easily learn the
419 linear correlation exhibiting in the rainfall-runoff process but failed to simulate the
420 dynamics of the system effectively. Therefore, the FFNN-ED model either seriously
421 over-estimated or under-estimated peak flow and had an obvious time-delay (time
422 shift) problem. As for the LSTM-ED model, the output flow value (e.g., $T+i$) of a
423 LSTM decoder is recurrently fed into the same decoder unit for making the forecast at
424 the next horizon (e.g., $T+i+1$). Therefore, the flow forecasts correlate with their
425 previous output flow. As described in Section 2.3, the process of information flow of
426 the LSTM structure is similar to the rainfall-runoff process. The forecast reliability of
427 the LSTM-ED model is significantly higher than that of the FFNN-ED model
428 throughout the rising limb, peak flow, and the recession limb of a flood. In short, the
429 LSTM-ED model not only achieves a better outcome than the FFNN-ED model in
430 simulating complex rainfall-runoff processes but also improves the reliability and
431 accuracy of multi-horizon forecasting of flood events.

432 **4.3 Impact assessment of input combination on model performance**

433 This study reduced the length of the input sequence and identified the impact of the
434 length reduction on the two ED models. Fig. 6 illustrates the $T+6$ forecast
435 performance of the FFNN-ED and LSTM-ED models with different input
436 combinations. The results show that the two models experience a continuous decrease
437 in performance as the length of the input sequence decreases, and this situation is
438 notably worse for the FFNN-ED model. The results of impact assessment show that
439 there is no significant difference in the performances of the LSTM-ED model with

440 input information spanning 8 (T-7, ..., 0) down to 5 (T-4, ..., 0) continuous hours.
441 Besides, the FFNN-ED model performs inferior to the LSTM-ED model under the
442 same scenarios. Comparing input information spanning 4 (T-3, ..., 0) and 8 (T-7, ..., 0)
443 continuous hours, the RMSE value increases by 20% while the R^2 and NSE values
444 decreases by 10% for the FFNN-ED model. In contrast, the RMSE value decreases by
445 10% while the R^2 and NSE values make no significant changes for the LSTM-ED
446 model. The results indicate that the LSTM-ED model is able to achieve similar
447 forecast performance with less input information while the FFNN-ED model does
448 have difficulty in making such achievement. This study speculates that this is because
449 the recurrent architecture of the LSTM unit feeds the next input vector with the output
450 vector of the previous unit such that the model can learn the temporal pattern in a
451 continuous way.

452

453 **5. Conclusions**

454 This study proposes a LSTM-based Encoder-Decoder (LSTM-ED) framework to
455 model multi-step-ahead flood forecasting. The results reveal that fusing the LSTM
456 unit with sequence-to-sequence learning into the ED model not only can improve the
457 accuracy and reliability of flood forecasting but also increase the interpretability of
458 the framework through translating the rainfall sequence to the runoff sequence.
459 Besides, the LSTM-ED model can better learn the rainfall-runoff process and provide
460 more reliable and accurate multi-step ahead forecasts than the FFNN-ED. The
461 findings of this study are summarized below.

462 (1) The FFNN-ED model can produce a small error and consume less time in
463 convergence during model training, but it suffers from unstable (wide variability)
464 and overfitting problems. The LSTM-ED model can reduce multi-step-ahead

465 forecast error and significantly mitigate the overfitting problem to provide more
466 stable performance. Still, it demands more time in training the model.

467 (2) In the flood forecasting of four test events, the time-delay at the horizon of 6
468 hours ahead (T+6) for the LSTM-ED model is much shorter than that of the
469 FFNN-ED model. The LSTM-ED model not only can make more accurate
470 forecasts on high flow of flood events induced by single-peak rainfall
471 distribution but also can make more stable forecasts on flood events induced by
472 multi-peak rainfall distribution, taking the FFNN-ED model as the benchmark.

473 (3) The LSTM-ED model plays an important role in modeling the rainfall-runoff
474 process for multi-step ahead flood forecasts, where the LSTM unit in the encoder
475 can effectively integrate sequential rainfall patterns with watershed discharge
476 while the LSTM decoder can systematically and precisely forecast the flow
477 sequence in a continuous way.

478 (4) According the impact assessment of the length of the input sequence on model
479 performance, the LSTM-ED model can produce much better performances than
480 the FFNN-ED model, especially when being fed with less input information.
481 This study speculates that this is because the architecture of the LSTM unit feeds
482 the next input vector with the output vector of the previous unit such that the
483 model can learn the temporal pattern in a continuous way.

484 A barrier to applying the ANNs (or DNNs) is their black-box nature that could
485 not provide explicit internal representation of hydrologic processes. In this study, the
486 input sequence was translated into the output sequence by configuring them into the
487 LSTM-based Encoder-Decoder learning framework and the implementation process
488 of the LSTM-ED model was linked with hydrological processes (i.e. the
489 rainfall-runoff process), as discussed briefly in Sect. 2.3.2. We believe that improving

490 the reliability and accuracy of model performance and increasing the interpretability
491 of the network internals would increase the trust in data-driven approaches and lead to
492 more practices in hydrologic sciences.

493 There are quite many sequence-to-sequence problems encountered in
494 hydrological fields. This study is only a case that applies the LSTM-ED to modeling
495 the rainfall-runoff problem. More extensive research on hydrological disasters (e.g.,
496 regional flooding or drought) and water resources management (e.g., inflow
497 forecasting and groundwater estimation) using the proposed methods can be explored
498 in the future.

499

500 **Acknowledgments**

501 The Ministry of Science and Technology supported this research, Taiwan (Grant
502 numbers: MOST 107-2621-M-002-004-MY3, and MOST 108-2911-I-002-507). The
503 data provides by the Northern Region Water Resources Office, Water Resources
504 Agency, Taiwan is much appreciated.

505

506 **References**

- 507 1. Abrahart, R. J., Heppenstall, A. J., See, L. M., 2007. Timing error correction
508 procedure applied to neural network rainfall—runoff modelling. *Hydrological
509 sciences journal* 52(3), 414-431.
- 510 2. Adikari, Y., Yoshitani, J. 2009. *Global Trends in Water-Related Disasters: An
511 Insight for Policymakers*, International Centre for Water Hazard and Risk
512 Management (ICHARM). The United Nations World Water Development Report
513 3, Tsukuba, Japan.
- 514 3. Audhkhasi, K., Rosenberg, A., Sethy, A., Ramabhadran, B., Kingsbury, B., 2017.

- 515 End-to-end ASR-free keyword search from speech. *IEEE Journal of Selected*
516 *Topics in Signal Processing* 11(8), 1351-1359.
- 517 4. Badrzadeh, H., Sarukkalige, R., Jayawardena, A. W., 2015. Hourly runoff
518 forecasting for flood risk management: Application of various computational
519 intelligence models. *Journal of Hydrology* 529, 1633-1643.
- 520 5. Bengio, S., Vinyals, O., Jaitly, N., Shazeer, N., 2015. Scheduled sampling for
521 sequence prediction with recurrent neural networks. In *Advances in Neural*
522 *Information Processing Systems*, 1171-1179.
- 523 6. Chandwani, V., Vyas, S. K., Agrawal, V., Sharma, G., 2015. Soft computing
524 approach for rainfall-runoff modelling: A review. *Aquatic Procedia* 4, 1054-1061.
- 525 7. Chang, F. J., Chen, P. A., Lu, Y. R., Huang, E., Chang, K. Y., 2014. Real-time
526 multi-step-ahead water level forecasting by recurrent neural networks for urban
527 flood control. *Journal of Hydrology* 517, 836-846.
- 528 8. Chang, F. J., Tsai, M. J., 2016. A nonlinear spatio-temporal lumping of radar
529 rainfall for modeling multi-step-ahead inflow forecasts by data-driven
530 techniques. *Journal of Hydrology* 535, 256-269.
- 531 9. Chang, L. C., Shen, H. Y., Chang, F. J., 2014. Regional flood inundation nowcast
532 using hybrid SOM and dynamic neural networks. *Journal of hydrology* 519,
533 476-489.
- 534 10. Chau, K. W., 2006. A review on integration of artificial intelligence into water
535 quality modelling. *Marine pollution bulletin* 52(7), 726-733.
- 536 11. Chen, P. A., Chang, L. C., Chang, F. J., 2013. Reinforced recurrent neural
537 networks for multi-step-ahead flood forecasts. *Journal of Hydrology* 497, 71-79.
- 538 12. Chiu, C. C., Sainath, T. N., Wu, Y., Prabhavalkar, R., Nguyen, P., Chen, Z.,
539 Kannan, A., Weiss, R. J., Rao, K., Gonina, E., Jaitly, N., Li, B., Chorowski, J.,

- 540 Bacchiani, M., 2018. State-of-the-art speech recognition with
541 sequence-to-sequence models. In 2018 IEEE International Conference on
542 Acoustics, Speech and Signal Processing, 4774-4778.
- 543 13. Costa-Jussa, M. R., 2018. From Feature to Paradigm: Deep Learning in Machine
544 Translation. *Journal of Artificial Intelligence Research* 61, 947-974.
- 545 14. Dawson, C. W., Wilby, R. L., 2001. Hydrological modelling using artificial neural
546 networks. *Progress in physical Geography* 25(1), 80-108.
- 547 15. Fengming, Z., Shufang, L., Zhimin, G., Bo, W., Shiming, T., Mingming, P., 2017.
548 Anomaly detection in smart grid based on encoder-decoder framework with
549 recurrent neural network. *The Journal of China Universities of Posts and*
550 *Telecommunications* 24(6), 67-73.
- 551 16. Freeman, B. S., Taylor, G., Gharabaghi, B., Thé, J., 2018. Forecasting air quality
552 time series using deep learning. *Journal of the Air & Waste Management*
553 *Association* 68(8), 866-886.
- 554 17. Hochreiter, S., Schmidhuber, J., 1997. Long short-term memory. *Neural*
555 *computation* 9(8), 1735-1780.
- 556 18. Humphrey, G. B., Gibbs, M. S., Dandy, G. C., Maier, H. R., 2016. A hybrid
557 approach to monthly streamflow forecasting: integrating hydrological model
558 outputs into a Bayesian artificial neural network. *Journal of hydrology* 540,
559 623-640.
- 560 19. Jeong, J., Park, E., 2019. Comparative applications of data-driven models
561 representing water table fluctuations. *Journal of Hydrology* 572, 261-273.
- 562 20. Kalteh, A. M., Hjorth, P., Berndtsson, R., 2008. Review of the self-organizing map
563 (SOM) approach in water resources: Analysis, modelling and application.
564 *Environmental Modelling & Software* 23(7), 835-845.

- 565 21. Kratzert, F., Klotz, D., Brenner, C., Schulz, K., Herrnegger, M., 2018.
566 Rainfall–runoff modelling using long short-term memory (LSTM) networks.
567 Hydrology and Earth System Sciences 22(11), 6005-6022.
- 568 22. Le, X. H., Ho, H. V., Lee, G., Jung, S., 2019. Application of Long Short-Term
569 Memory (LSTM) Neural Network for Flood Forecasting. Water 11(7), 1387.
- 570 23. Liu, W., Wang, Z., Liu, X., Zeng, N., Liu, Y., Alsaadi, F. E., 2017. A survey of
571 deep neural network architectures and their applications. Neurocomputing 234,
572 11-26.
- 573 24. Lohani, A. K., Goel, N. K., Bhatia, K. K. S., 2014. Improving real time flood
574 forecasting using fuzzy inference system. Journal of hydrology 509, 25-41.
- 575 25. Malinowski, M., Rohrbach, M., Fritz, M., 2017. Ask your neurons: A deep
576 learning approach to visual question answering. International Journal of Computer
577 Vision 125(1-3), 110-135.
- 578 26. Marmanis, D., Schindler, K., Wegner, J. D., Galliani, S., Datcu, M., Stilla, U.,
579 2018. Classification with an edge: improving semantic image segmentation with
580 boundary detection. ISPRS Journal of Photogrammetry and Remote Sensing 135,
581 158-172.
- 582 27. Noori, N., Kalin, L., 2016. Coupling SWAT and ANN models for enhanced daily
583 streamflow prediction. Journal of Hydrology 533, 141-151.
- 584 28. Nourani, V., Komasi, M., 2013. A geomorphology-based ANFIS model for
585 multi-station modeling of rainfall–runoff process. Journal of Hydrology 490,
586 41-55.
- 587 29. Nourani, V., Baghanam, A. H., Adamowski, J., Kisi, O., 2014. Applications of
588 hybrid wavelet–artificial intelligence models in hydrology: a review. Journal of
589 Hydrology 514, 358-377.

- 590 30. Nourani, V., 2017. An emotional ANN (EANN) approach to modeling
591 rainfall-runoff process. *Journal of Hydrology* 544, 267-277.
- 592 31. Nourani, V., Sattari, M. T., Molajou, A., 2017. Threshold-based hybrid data
593 mining method for long-term maximum precipitation forecasting. *Water*
594 *Resources Management* 31(9), 2645-2658.
- 595 32. Nourani, V., Elkiran, G., & Abdullahi, J., 2020. Multi-step ahead modeling of
596 reference evapotranspiration using a multi-model approach. *Journal of Hydrology*
597 581, 124434.
- 598 33. Nourani, V., Molajou, A., Uzelaltinbulat, S., Sadikoglu, F., 2019. Emotional
599 artificial neural networks (EANNs) for multi-step ahead prediction of monthly
600 precipitation; case study: northern Cyprus. *Theoretical and Applied Climatology*,
601 1-16.
- 602 34. Nourani, V., Partoviyani, A., 2018. Hybrid denoising-jittering data pre-processing
603 approach to enhance multi-step-ahead rainfall-runoff modeling. *Stochastic*
604 *environmental research and risk assessment* 32(2), 545-562.
- 605 Kingsbury, B., Saon, G., Soltau, H., Mohamed, A. R., Dahl, G., Ramabhadran, B.,
606 2015. Deep convolutional neural networks for large-scale speech tasks. *Neural*
607 *Networks* 64, 39-48.
- 608 35. Sezen, C., Bezak, N., Bai, Y., Šraj, M., 2019. Hydrological modelling of karst
609 catchment using lumped conceptual and data mining models. *Journal of*
610 *Hydrology* 576. 98-110.
- 611 36. Shafaei, M., Adamowski, J., Fakheri-Fard, A., Dinpashoh, Y., Adamowski, K.,
612 2016. A wavelet-SARIMA-ANN hybrid model for precipitation forecasting.
613 *Journal of Water and Land Development* 28(1), 27-36.
- 614 37. Shenify, M., Danesh, A. S., Gocić, M., Taher, R. S., Wahab, A. W. A., Gani, A.,

- 615 Shamshirband S., Petković, D., 2016. Precipitation estimation using support
616 vector machine with discrete wavelet transform. *Water resources management*
617 30(2), 641-652.
- 618 38. Shoaib, M., Shamseldin, A. Y., Khan, S., Khan, M. M., Khan, Z. M., Sultan, T.,
619 Melville, B. W., 2018. A comparative study of various hybrid wavelet feedforward
620 neural network models for runoff forecasting. *Water resources management* 32(1),
621 83-103.
- 622 39. Sutskever, I., Vinyals, O., Le, Q. V., 2014. Sequence to sequence learning with
623 neural networks. In *Advances in neural information processing systems*,
624 3104-3112.
- 625 40. Tan, Q. F., Lei, X. H., Wang, X., Wang, H., Wen, X., Ji, Y., Kang, A. Q., 2018. An
626 adaptive middle and long-term runoff forecast model using EEMD-ANN hybrid
627 approach. *Journal of hydrology* 567, 767-780.
- 628 41. Taormina, R., Chau, K. W., & Sivakumar, B., 2015. Neural network river
629 forecasting through baseflow separation and binary-coded swarm optimization.
630 *Journal of Hydrology* 529, 1788-1797.
- 631 42. Tsai, M. J., Abrahart, R. J., Mount, N. J., Chang, F. J., 2014. Including spatial
632 distribution in a data- driven rainfall- runoff model to improve reservoir inflow
633 forecasting in Taiwan. *Hydrological Processes* 28(3), 1055-1070.
- 634 43. Valipour, M., 2016. Optimization of neural networks for precipitation analysis in a
635 humid region to detect drought and wet year alarms. *Meteorological Applications*
636 23(1), 91-100.
- 637 44. Venugopalan, S., Rohrbach, M., Donahue, J., Mooney, R., Darrell, T., Saenko, K.,
638 2015. Sequence to sequence-video to text. In *Proceedings of the IEEE*
639 *international conference on computer vision*, 4534-4542.

- 640 45. Wiseman, S., Rush, A. M., 2016. Sequence-to-sequence learning as beam-search
641 optimization. arXiv 1606.02960v2.
- 642 46. Zhang, J., Zhu, Y., Zhang, X., Ye, M., Yang, J., 2018. Developing a Long
643 Short-Term Memory (LSTM) based model for predicting water table depth in
644 agricultural areas. *Journal of Hydrology* 561, 918-929.
- 645 47. Zhou, Y., Chang, F. J., Chang, L. C., Kao, I. F., Wang, Y. S., 2019. Explore a deep
646 learning multi-output neural network for regional multi-step-ahead air quality
647 forecasts. *Journal of Cleaner Production* 209, 134-145.
- 648 48. Zhu, L., Xu, Z., Yang, Y., Hauptmann, A. G., 2017. Uncovering the temporal
649 context for video question answering. *International Journal of Computer
650 Vision* 124(3), 409-421.
- 651 49. Zhu, Y., Zabararas, N., 2018. Bayesian deep convolutional encoder–decoder
652 networks for surrogate modeling and uncertainty quantification. *Journal of
653 Computational Physics* 366, 415-447.
- 654

Credit Author Statement

Conceptualization: I-Feng Kao, Li-Chiu Chang, Fi-John Chang;

Data curation: I-Feng Kao, Li-Chiu Chang;

Formal analysis: I-Feng Kao, Yanlai Zhou, Li-Chiu Chang, Fi-John Chang;

Funding acquisition: Fi-John Chang, Li-Chiu Chang;

Investigation: Fi-John Chang, Li-Chiu Chang;

Methodology: I-Feng Kao, Yanlai Zhou;

Project administration: Fi-John Chang;

Resources: I-Feng Kao;

Software: I-Feng Kao, Li-Chiu Chang;

Supervision: Fi-John Chang, Li-Chiu Chang;

Validation: I-Feng Kao, Yanlai Zhou;

Visualization: I-Feng Kao;

Roles/Writing - original draft: I-Feng Kao;

Writing - review & editing: Fi-John Chang

Declaration of interests

The authors declare that they have no known competing financial interests or personal relationships that could have appeared to influence the work reported in this paper.

The authors declare the following financial interests/personal relationships which may be considered as potential competing interests: